Collapse of Long Cylindrical Shells under Combined Bending and Pressure Loads

WENDELL B. STEPHENS* AND JAMES H. STARNES, JR.†
NASA Langley Research Center, Hampton, Va.

AND

B. O. ALMROTH‡
Lockheed Palo Alto Research Laboratory, Palo Alto, Calif.

The nonlinear collapse behavior of long cylindrical shell structures subject to a bending load only or combined bending and uniform normal pressure loads is studied using the STAGS computer code. Two modes of nonlinear collapse are investigated to determine maximum strength. One mode of collapse is described by circumferential flattening of the cylinder cross section and the other mode is represented by axial wrinkling in the region of maximum compression. Results compare favorably with available published data for cylinders loaded by pure bending and results are presented for combined loads which have not been previously reported. The collapse loads obtained in this study show that current design criteria are conservative except for a narrow range of length-to-radius ratios and pressures.

Nomenclature

A	= area of ring cross section
a	= amplitude of axial wrinkle (wave)
E	= modulus of elasticity
I	= cross-sectional ring moment of inertia about centroidal axis normal to the plane of ring
L	= length of cylinder
$M_{cr} = 0.6\pi rt^2E$	
$M = \pi r^2N$	= applied bending moment
$\bar{M}$	= Brazier collapse bending moment for cylinders of infinite length
N	= amplitude of applied end load
N_{cr}	= classical uniform axial buckling load per unit length
N_x	= axial stress resultant
n	= number of circumferential waves in initial imperfection
p	= uniform normal pressure (positive for internal pressures)
p_{cr}	= classical uniform buckling pressure
p_e	= magnitude of linear bifurcation buckling pressure of an elastically restrained cylinder due to a uniform external pressure
$R_b = M/M_{cr}$	= ratio of collapse bending moment for cylinder subjected to combined loads to the allowable bending moment for the cylinder when subjected only to bending
$R_p = p/p_e$	= ratio of pressure on cylinder subjected to combined loads to the allowable external pressure for the cylinder when subjected only to external pressure
r	= radius of cylinder
t	= thickness of cylinder
w	= normal displacement
w_i	= initial imperfection in shell reference surface
w_o	= maximum imperfection amplitude
Δw	= maximum change in cylinder diameter at mid-length during loading
δw	= difference in displacement w between datum displacement and a higher-load-state displacement
x, θ	= axial and circumferential coordinates
γ	= correlation factor between experimental results and classical theory
λ	= imperfection axial half-wave length
ν	= Poisson's ratio
$\bar{\sigma}$	= maximum compressive axial stress at collapse
$\sigma_{cr} = 0.6Et/r$	= classical compressive buckling stress due to a uniform axial load for $\nu = 0.3$

Received April 15, 1974; presented as Paper 74-407 at the AIAA/ASME/SAE 15th Structures, Structural Dynamics and Materials Conference, Las Vegas, Nevada, April 17–19, 1974; revision received August 19, 1974.

Index category: Structural stability analysis.

* Aerospace Engineer, Structural Mechanics Branch, Structures and Dynamics Division. Member AIAA.

† Aerospace Engineer, Computer Aided Methods Branch, Structures and Dynamics Division. Member AIAA.

‡ Senior Staff Scientist. Member AIAA.

Introduction

A STUDY of the nonlinear behavior to collapse of shell structures subject to a bending load only or combined bending and uniform normal pressure is a complex problem even for shells of simple geometry. The cylindrical shell subject to bending has been studied by several researchers and yet there is still no design data applicable to a long shell with combined bending and pressure loads. Brazier[1] was able to predict the critical bending moment for the collapse of an infinitely long cylinder by deriving an expression for the total strain energy per unit length of the shell in terms of the change in axial curvature. By minimizing this expression with respect to the change in curvature, Brazier found the critical or collapse bending moment $\bar{M}$ to be

$$\bar{M} = \frac{2(2)^{1/2}}{9}\frac{E\pi rt^2}{(1-\nu^2)^{1/2}}$$

which occurred when the flattening of the cross section Δw reached

$$\Delta w = (2/9)r$$

Here E is the modulus of elasticity, ν is Poisson's ratio, r is the radius of the cylinder, and t is the thickness of the cylinder. If the axial stress at collapse $\bar{\sigma}$ due to bending is computed using the undistorted cross-sectional properties of the cylinder and the value of ν is taken to be equal to 0.3 then

$$\bar{\sigma} = 0.33Et/r$$

Seide and Weingarten[2] predicted the bifurcation buckling load by using a linear membrane prebuckling state for finite-length, simply supported cylinders loaded by pure bending. Their results

showed that the critical maximum axial stress due to bending is, for all practical purposes, equal to the critical compressive stress for uniform axial compression and, therefore, can be approximated by the classical expression for uniform axial compression

$$\sigma_{cr} = 0.6Et/r$$

A paper by Aksel'rad[3] reports an improvement of this bifurcation buckling study by simultaneously including the effects of edge constraints and geometric nonlinearities in the prebuckling state. Aksel'rad's solution of the nonlinear prebuckling is based on an asymptotic expansion and his solution of bifurcation into a wavy mode is based on an analogy with circular cylindrical shells loaded with uniform axial compression. Aksel'rad reports that the collapse stress varies from a value of $0.6Et/r$ for short cylinders to a value of $0.295Et/r$ for shells with a length-to-radius ratio greater than $2.5(r/t)^{1/2}$. A more rigorous solution by Almroth and Starnes[4] using a nonlinear analysis essentially verifies Aksel'rad's results and shows them to be reasonably accurate.

The purpose of this paper is to investigate the effects of combined bending and external or internal pressure loads on the collapse of cylindrical shells by taking nonlinear effects into account. Understanding the effects of combined loads on shell behavior is important in the study and design of pressurized tanks and other shell components in aircraft and spacecraft structures, as well as in submerged pipelines.

Analysis

Computer Program

The STAGS code (Structural Analysis of General Shells)[5,6] is used in this study to perform the analyses. STAGS is a general-purpose computer program for analyzing shells. It is based on a two-dimensional finite-difference approximation of the total potential energy expression which retains the accuracy of shell theory and is capable of determining both bifurcation buckling loads based on a linear prebuckling state and nonlinear collapse loads. By including a small imperfection in the nonlinear analysis, a bifurcation buckling load based on a nonlinear prebuckling state can also be estimated.

If there are two loads, the loads may be incremented independently. For the results presented herein, the pressure is incremented to a prescribed value while the value of the moment is small (and the response of the shell to the combined loads is expected to be linear). The pressure is then held constant at its prescribed value while the moment is incrementally increased into the nonlinear range until collapse occurs.

Description of the Model

The model chosen for this study is an isotropic cylinder with the following basic geometric and material properties: $r/t = 100$, $E = 6.895$ kPa (10^7 psi), and $\nu = 0.3$. The length-to-radius ratio L/r is the geometric parameter varied in the study. The loading and shell geometry are shown in Fig. 1. The applied end load N_x that generates the bending moment M is $N_x = -N\cos\theta$, where N is the amplitude of the applied load and θ is the circumferential coordinate. The bending moment is given by $M = N\pi r^2$. Note that the applied normal pressure p is considered positive outward.

In this study only one-quarter of a shell is analyzed due to a plane of symmetry normal to the cylinder axis at mid-length and an axial plane of symmetry passing through the

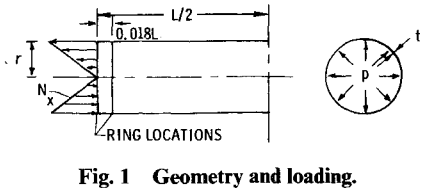

Fig. 1 Geometry and loading.

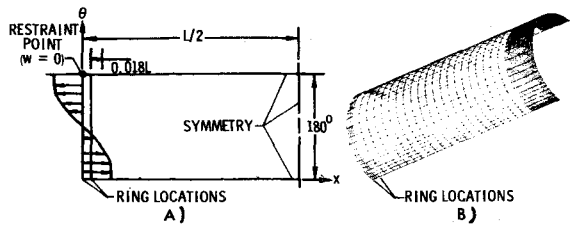

Fig. 2 Analytical model. a) Developed view. b) Isometric view, finite-difference spacing.

points of maximum bending load. The one-quarter shell segment analyzed is shown in both developed and isometric views in Fig. 2. Symmetry conditions are applied at three boundaries as shown in Fig. 2(a). The remaining boundary is elastically restrained by two end rings. These rings are stiff enough to approximate a condition for which the end plane rotates and translates with undistorted cross section and with a minimum of warping of the cross section. In the analytical model, the end rings are located at x equal to 0, and $0.018L$. For the rings, $A/r^2 = 0.02$ and $I/r^4 = 0.0002$, where A is the cross-sectional area of the ring and I is the cross-sectional moment of inertia about the centroidal axis normal to the plane of the ring. In calculating elastic properties, other cross-sectional moments of inertia of the rings were considered zero and the torsional stiffness was considered zero. Rigid body motion is prevented by requiring that the normal displacement w equals zero at a point with coordinates (0, 180°).

Antisymmetry along the axial edges of the model was not considered in this study since such conditions would leave node lines at points of maximum stress. Symmetry conditions are believed to be an accurate physical representation at these boundaries.

The finite-difference grid spacing is varied in both the axial and circumferential directions to allow a concentration of mesh points in regions where failure is expected, and the grid point spacing is shown on the quarter panel in Fig. 2(b). The 50 by 21-grid point network shown represents the minimum number of grid points used in the study.

In order to permit bifurcation buckling from the nonlinear state, a small imperfection is introduced. The imperfection w_i used in this study is defined as

$$\frac{w_i}{t} = \frac{w_o}{t}\cos\left(\pi\frac{(L/2-x)}{\lambda}\right)\cos\left(\frac{n\pi}{180^\circ}\theta\right)$$

where $w_o/t = 10^{-3}$, $\lambda/L = 0.017$, and

$$n = \begin{cases} 3 \text{ for } 6 \leqq L/r \leqq 15 \\ 2 \text{ for } L/r = 20 \end{cases}$$

Here w_o and λ are the imperfection amplitude and axial half-wave length, respectively, and n is the number of circumferential waves of the imperfection.

Types of Failure

Prior to collapse, general deformations are allowed. It has been observed that collapse is either of two failure modes: Brazier flattening (cross-sectional or circumferential flattening) and short-wave axial buckling (bifurcation buckling collapse based on a nonlinear prebuckling state). To facilitate the determination of the collapse load, attention was focused on one or the other of these two collapse mechanisms. Although these modes occur simultaneously, one or the other will predominate at collapse. The criteria used, in each case, to determine collapse is discussed using illustrative examples.

The nonlinear collapse load that corresponds to Brazier flattening is determined from a graph such as that presented in Fig. 3 where the applied bending moment M is plotted as a function of the cross-sectional flattening $\Delta w/t$. The cross-sectional flattening is defined in Fig. 3 to be

$$\Delta w/t = -1/t[w(L/2, 0) + w(L/2, 180^\circ)]$$

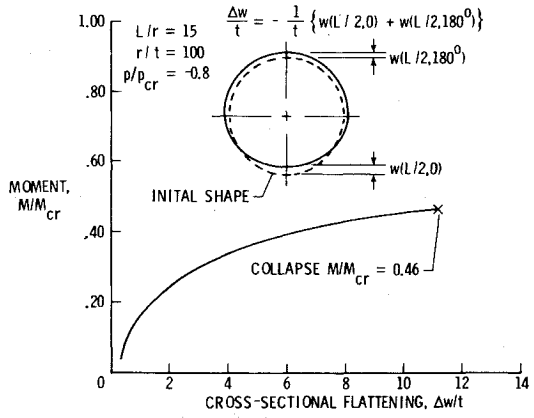

Fig. 3 Determination of collapse moment using Brazier flattening of cylinder cross section at midlength.

The ordinate is defined by the ratio of M/M_{cr} where $M_{cr} = 0.6\pi rt^2E$ which corresponds to an applied load amplitude of $N = 0.6(Et^2/r)$ when $\nu = 0.3$. The particular cylinder chosen for the illustrative example in Fig. 3 has the geometric properties of L/r equal to 15 and r/t equal to 100, and an external pressure of $-0.8p_{cr}$. The classical buckling pressure p_{cr} of a simply supported cylinder loaded with a uniform external pressure is given in Ref. 7 as

$$p_{cr} = 0.926Et^{5/2}/(r^{3/2}L)$$

for $\nu = 0.3$. The nonlinear behavior can be described by means of a curve relating the applied moment M to the cross-sectional flattening. The Brazier collapse load is defined as the load at which the slope of the curve approaches zero. Collapse is assumed to occur when appreciable increases in Δw occur for increases of load of the order of 0.01%. In this example, collapse occurs at a value of M/M_{cr} equal to 0.46. The inset in Fig. 3 shows the deformation of the cylinder cross section at a load state near collapse.

The nonlinear collapse load that corresponds to the short-wave axial buckling mode is defined by means of the horizontal tangent of a curve relating the applied bending moment to the growth of a wrinkle (or wavy mode) in the axial direction. Generally, this axial wrinkle does not begin to develop until a considerable amount of bending moment has been applied. The procedure for determining short-wave axial buckling loads is illustrated in Fig. 4 for a cylinder with geometric properties of L/r of 10 and r/t of 100, and an external pressure equal to $-0.5p_{cr}$. Usually, the wrinkling mode is not easily detected since its amplitude is small in comparison to other shell deformations. Therefore, to detect wrinkling, it is convenient to take a displacement state at a load level near where wrinkling is suspected to have been initiated and use that displacement state as a datum state. This datum state is subtracted from all subsequent displacement fields at the higher load levels. This difference δw in the normal displacements is calculated at the meridian of maximum compression and is plotted as a function of axial distance in Fig. 4(a) where an axial wave of amplitude a is shown to be developing near the midlength of the cylinder. The applied bending moment is then plotted as a function of the amplitude of the wave as shown in Fig. 4(b). If this moment vs amplitude curve approaches a horizontal tangent, then a mode of collapse has occurred which is called the short-wave axial buckling mode in this study. After wrinkling starts to develop, the wrinkle amplitude increases rapidly with small increases in load. The rapid growth, although not a true bifurcation, may be considered to indicate that bifurcation based on a nonlinear prebuckling state would have occurred near this load if no imperfections were present. Collapse is assumed to occur when relatively large increases in amplitude occur for increases of moment of the order of 0.01%. Buckling, and therefore collapse, for this particular example occurs at approximately a value of M equal to $0.636M_{cr}$.

The collapse of the cylinder is determined by monitoring both of these modes. The predominant mode that causes collapse is the one that first approaches a horizontal tangent. However, in general, these modes are coupled. This coupling of buckling phenomena is a major reason why the nonlinear analysis of even simple shell geometries is often difficult.

Results and Discussion

All results presented are for cylinders with r/t equal to 100. Collapse moments are obtained for cylinders with L/r values of 6, 10, 15, and 20 with p/p_{cr} equal to 3.0, 1.0, 0.0, -0.5, -0.8, and -0.9. Bending moments are presented as a function of Brazier flattening for p/p_{cr} equal to 0.0, 3.0, and -0.9. Stress distributions at the shell midlength near collapse load are presented and discussed. A summary of results for collapse moments is presented and compared with design criteria interaction curves.

Pure Bending

Results for unpressurized long cylinders are presented and compared with the classical solutions[1,2] in Fig. 5. The dashed curves show the moment plotted as a function of cross-sectional flattening for various values of the length-to-radius ratios. Some of these results were first presented in Ref. 4. The envelope of the collapse moments is shown by the solid curve. It is seen that this envelope approaches both the expected classical value of M equal to M_{cr} for short cylinders and the Brazier solution of $0.55M_{cr}$ at $\Delta w/r$ equal to 2/9 (or $\Delta w/t$ equal to 22.2). Collapse for these results is due to an interaction between the Brazier effect and the short-wave axial buckling mode, although Brazier flattening becomes the dominant effect as values of L/r increase.

Combined Bending and Internal Pressure

A comparison is made for the collapse moments of cylinders of various lengths for a relatively high value of internal pressure of p/p_{cr} equal to 3.0 in Fig. 6. Again, the dashed curves represent the moment as a function of cross-sectional flattening

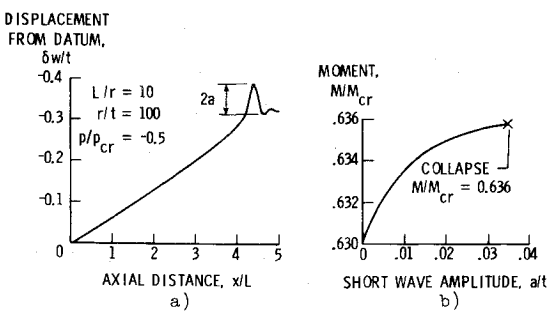

Fig. 4 Determination of collapse load for axial short-wave failure mode of cylinder.

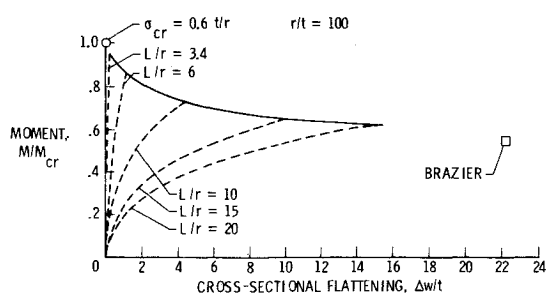

Fig. 5 Comparison of collapse moments of unpressurized cylinders with classical results.

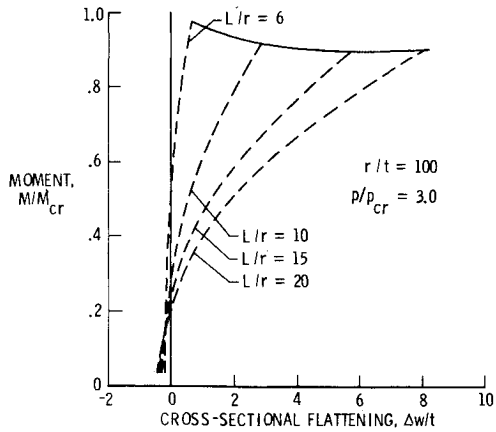

Fig. 6 Comparison of collapse moments of cylinders with combined bending and internal pressure.

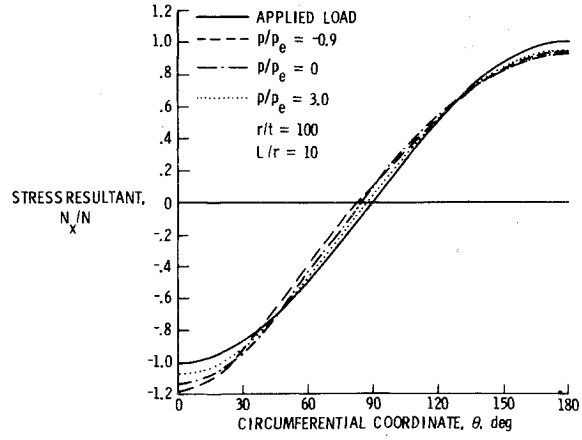

Fig. 8 Variation of stress resultant at collapse for a long cylinder with combined bending and pressure.

for various L/r values and the solid curve is the envelope of the collapse moments. In each case cross-sectional flattening is inhibited by the internal pressure, and thus the bending load capacity is increased. The collapse loads generally decrease as values of L/r increase. However, the collapse load for a cylinder with an L/r of 20 is found to be slightly above that of one with an L/r of 15. An explanation of this behavior requires further investigation.

Combined Bending and External Pressure

The same shell geometries are considered again in Fig. 7 for a pressure (external) of $-0.9p_{cr}$. Again, the dashed curves represent the moment as a function of cross-sectional flattening for various L/r values and the solid curve is the envelope of the collapse moments. The effects of external pressure and applied moment reinforce one another while causing the flattening of the cylinder. In the case of L/r equal to 20 collapse occurs as a result of Brazier flattening. Collapse is attributed to short-wave axial wrinkling for the smaller values of L/r shown in the figure. The dashed curve for L/r equal to 6 initially shows an increase in the cross-section diameter. This phenomenon occurs because the normal displacement for the applied pressure and small applied moment loading approximates a distorted n equal to 3 circumferential distribution. As the moment increases, however, the circumferential displacement pattern gradually transforms into the expected oval configuration. This behavior also occurs to lesser extents in the analyses for p/p_{cr} equal to -0.5 and -0.8 when L/r is equal to 6.

Axial Stress Resultants at Midlength

The axial stress resultant distribution at the cylinder midlength is shown for a load near the collapse loads in Fig. 8 for pressures of $-0.9p_{cr}$, 0.0, and $3.0p_{cr}$, respectively, and a cylinder of length-to-radius ratio of 10. The applied load at the edge of the cylinder is a cosine curve and is shown as a solid line. The dash-dot curve represents the stress distributions for $p/p_{cr} = 0$. For this case the peak compressive stress increase at midlength is about 13% greater than the applied stress resultant and the zero stress level occurs at $\theta = 84°$ (instead of at 90°). The stress resultant for a large internal pressure level of $p/p_{cr} = 3.0$ is shown by the dotted curve. Here the peak compressive stress increases only 7% above the applied stress resultant and the zero stress level occurs at $\theta = 87°$. This relatively small phase shift indicates in the latter case a relatively small shift in the neutral axis location which suggests that internal pressure does indeed inhibit flattening. The stress resultant for a large external pressure level of $p/p_{cr} = -0.9$ is shown by the dashed curve. Here the maximum compressive stress increase is approximately 18% above the applied stress and the zero stress level occurs at $\theta = 84°$. Although the location of the neutral axis at collapse is essentially the same as for the unpressurized case, the relatively large increase in compressive stress indicates that external pressures tend to accentuate the Brazier effect.

Summary of Collapse Moments

A summary of the collapse moment curves obtained for all pressure levels and L/r ratios studied (including those of Figs. 5–7) is shown in Fig. 9. The collapse moments are plotted as a function of cross-sectional flattening. The solid curves correspond to constant pressure levels and the dashed curves correspond to constant L/r values. For an internal pressure of $3.0p_{cr}$ the collapse moments approach the limiting value of M_{cr}. As the pressure parameter decreases to the value of $-0.9p_{cr}$ relatively small changes in p (compared to p_{cr}) produce large changes in collapse moment. A large portion of these collapse curves show that failure occurs well below the Brazier collapse

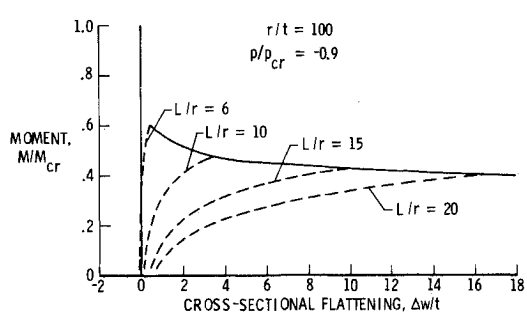

Fig. 7 Comparison of collapse moments of cylinders with combined bending and external pressure.

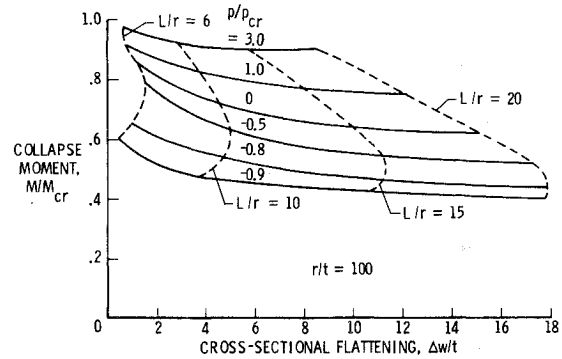

Fig. 9 Comparison of collapse moments of cylinders with combined bending and pressure.

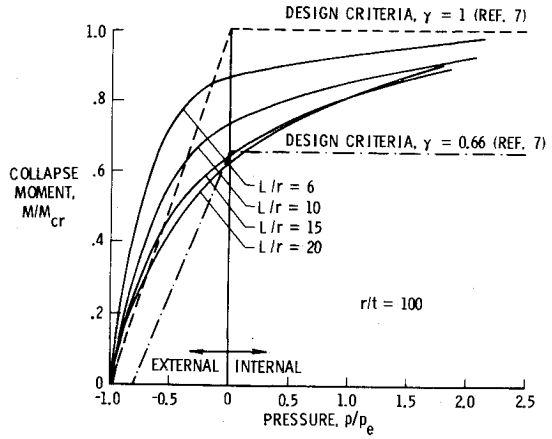

Fig. 10 Interaction curves for the collapse of cylindrical shells under bending and pressure.

value for unpressurized cylinders of $0.55M_{cr}$. In each case the constant pressure curves tend toward a limit for the collapse moments which is dependent on the pressure level. The constant L/r curves in Fig. 9 are all nonlinear in character with large internal pressures inhibiting the amount of flattening. The results for large external pressures also show a decrease in cross-sectional flattening at collapse in Fig. 9. This decrease in flattening at collapse, however, is not due to a decrease in the dominance of the Brazier collapse mode. Instead, it is attributed to the relatively large compressive stress buildup at the cylinder midlength caused by the combined loads of bending and external pressure. This stress buildup causes the moment vs flattening curves to tend toward a maximum because the Brazier-type collapse mode is becoming more dominant (e.g., compare Figs. 6 and 7) as both external pressure and L/r parameter increase.

Interaction Curves

The existing design criteria for interaction curves[7,8] for combinations of loading conditions which may cause buckling specifies that the sum of the critical load ratios is equal to unity. For combined bending and external pressure loads, the interaction curve is expressed by the linear relation $R_b + R_p = 1$, where R_b is the ratio of the collapse bending moment for the cylinder subject to combined loads to the allowable bending moment for the cylinder when subjected only to bending and therefore $R_b = M/M_{cr}$.

Similarly, R_p is the ratio of the pressure on the cylinder subjected to combined loads to the allowable external pressure for the cylinder when subjected only to external pressure. Here R_p is given by $R_p = p/p_e$, where p_e is the buckling pressure for cylinders with the elastic end ring restraint described previously. For internal pressure, the contribution of R_p is neglected. The buckling pressure p_e is determined with the STAGS code using a linear bifurcation buckling analysis and the results for the L/r values used in this study are given in the following table:

Table 1 Linear bifurcation buckling values for elastically restrained cylinders loaded by external pressure; $r/t = 100$

L/r	p_e/p_{cr}
6	1.395
10	1.446
15	1.612
20	1.665

These substantial differences between the values of p_e and p_{cr} are similar to those reported by Sobel[9] for hydrostatically loaded cylinders. He found that the buckling strength based on a linear membrane prebuckling state of cylinders with clamped edges (and with $L/r \leq 10$) was as much as 50% greater than those for cylinders with simply supported edges. The interaction curves for all results studied are presented in Fig. 10 where M/M_{cr} is plotted as a function of p/p_e. The solid curves correspond to collapse moments at constant values of L/r. The dashed curve which passes through the points of M/M_{cr} and p/p_e equal to unity is the design criteria relation discussed previously. In practical applications, a conservative design requires the use of an empirical factor γ which correlates experimental results with theoretical results. These differences in experimental and theoretical results are believed to be primarily due to small initial geometric imperfections. In Ref. 7 it is recommended that M_{cr} be multiplied by γ and p_e be multiplied by $\gamma^{1/2}$. For r/t of 100 the value of γ is 0.66. Using this factor, the design criteria curve is replotted and is shown by the dash-dot curve. For a conservative design, this curve should represent a lower bound to the analytical results, and indeed it does except for a small region for large L/r values around zero pressure. This small discrepancy is not too surprising since the experimental data used to determine the empirical factor γ is based on studies using lower L/r values than those studied herein. A comparison of the analytical results with the design curve at γ equal to unity show large differences for all L/r values. In each case this design criterion is unconservative throughout the range of internal pressures and, in most cases, well into the range of external pressures. For large external pressures this criterion is conservative. Thus, the nonlinear analysis yields results that correspond to a behavior which is quite different from the criterion. The interaction curves for the nonlinear results also show a large variation with respect to L/r values which is not reflected in the design criterion. This variation seems reasonable since the dominance of Brazier flattening increases as L/r values increase. Curves for higher L/r values should show better agreement with the design curve corrected by the empirical factor since the Brazier flattening mode is expected to be less susceptible to initial imperfections than the short-wave axial buckling mode. For example, at L/r equal to 10 and p/p_e equal to zero, M/M_{cr} is 0.73 or 11% greater than the lower bound design curve. For internal pressures this difference increases to 37% and correspondingly, Brazier flattening is inhibited and the structure is expected to be more imperfection sensitive since the axial short wave is dominant. For external pressures, the converse argument holds and the analytical results and the design criterion tend to converge and Brazier flattening is dominant. As the external pressure approaches p_e the buckling mode becomes that for pressure only and the nonlinearities of the prebuckling state have a negligible effect.

Conclusion

Analyses for the nonlinear collapse of isotropic cylinders with a radius-to-thickness ratio of 100 and loaded by either bending or combined bending and pressure loads are performed. Two modes of failure are investigated: circumferential or Brazier flattening and a nonlinear axial wrinkling. Results for cylinders loaded by pure bending are in agreement with previously published data and new results are presented for cylinders under combined loads of bending and internal or external pressure.

As the internal pressure level is increased, the collapse moment increases and approaches the limiting value of M_{cr}. As the external pressure is increased, the collapse moment is decreased in a number of cases to a value well below the Brazier collapse moment for unpressurized cylinders.

Interaction curves are presented for combinations of collapse moment and pressure loads and are found to vary as a function of L/r. The lower L/r values considered show the largest differences from conventional design criteria which take into account an experimental correlation factor. In these cases short-wave axial buckling modes (which tend to be imperfection sensitive) are more dominant than for higher L/r values. For

higher L/r values, Brazier flattening (which tends to be imperfection insensitive) is accentuated and agreement with the design criteria correlated with experiment is better.

References

[1] Brazier, L. G., "On the Flexure of Thin Cylindrical Shells and Other 'Thin' Sections," *Proceedings of the Royal Society, Series A*, Vol. CXVI, 1926, pp. 104–114.

[2] Seide, P., and Weingarten, V. I., "On the Buckling of Circular Cylindrical Shells Under Pure Bending," *Journal of Applied Mechanics*, Vol. 28, 1961, pp. 112–116.

[3] Aksel'rad, E. L., "Refinement of the Upper Critical Loading of Pipe Bending Taking Account of the Geometrical Nonlinearity" (in Russian), *Izvestiia, AN, SSSR, OTN, Mekhanika i Mashinostroenie*, No. 4, 1965, pp. 123–139.

[4] Almroth, B. O., and Starnes, James H., Jr., "The Computer in Shell Stability Analysis," *presented at the 1973 ASCE National Structural Engineering Meeting*, San Francisco, Calif., April 9–13, 1973.

[5] Almroth, B. O., Brogan, F. A., and Marlowe, M. B., "Collapse Analysis for Shells of General Shape," *Vol. I: Analysis*, AFFDL–TR–71–8, Aug. 1972, Air Force Flight Dynamics Lab., Wright-Patterson Air Force Base, Ohio.

[6] Almroth, B. O., Brogan, F. A., Meller, E., Zele, F., and Peterson, H. T., "Collapse Analysis for Shells of General Shape, Vol. II, User's Manual for the STAGS-A Computer Code," AFFDL–TR–71–8, March 1973.

[7] *Buckling of Thin-Walled Circular Cylinders*, SP–8007, Aug. 1968, NASA.

[8] Baker, E. H., Cappelli, A. P., Kovalevsky, L., Rish, F. L., and Verette, R. M., "Shell Analysis Manual," CR–912, April 1968, NASA.

[9] Sobel, L. H., "Effects of Boundary Conditions on the Stability of Cylinders Subject to Lateral and Axial Pressures," *AIAA Journal*, Vol. 2, No. 8, Aug. 1964, pp. 1437–1440.

JANUARY 1975 AIAA JOURNAL VOL. 13, NO. 1

Nonstationary Spectral Analysis for Linear Dynamic Systems

W. R. DAVIS JR.*
Air Force Flight Dynamics Laboratory, Wright-Patterson Air Force Base, Ohio
AND
L. L. BUCCIARELLI JR.†
Smithsonian Institution, Washington, D.C.

Second-order statistics of nonstationary processes in the form of time dependent spectra are studied with emphasis on "instantaneous" and "evolutionary" spectral densities. An integrated procedure for the time dependent spectral response calculation for linear systems with digital analysis of input data is presented for excitation processes in the form of a product of a deterministic envelope and a stationary random process. The envelope is approximated using a finite sum Fourier series, the Fourier coefficients being estimated directly from input time records. An example, using artificial earthquake motions, illustrates the procedure.

Nomenclature

$A(t, \omega)$ = envelope function [see Eq. (11)]
a_m = Fourier coefficient of $c(t)$
b = bias error
$c(t)$ = envelope function [see Eq. (1)]
c_m = measured Fourier coefficient of $c(t)$
$d(t)$ = measured estimate of $c(t)$
$f_y(t, \omega)$ = evolutionary spectral density of process y
$H(\omega)$ = Fourier transform of $h(t)$
$h(t)$ = impulse response of time invariant linear system
i = $(-1)^{1/2}$
M = number of sampled points in discrete Fourier transform
N = number of realizations in experimental average
$n(t)$ = stationary random process
R = order of Fourier series approximation
$R_n(t)$ = autocorrelation of process n
$\hat{R}_n(t)$ = normalized autocorrelation [see Eq. (29)]
r = frequency resolution parameter [see Eq. (33)]
$S_n(\omega)$ = spectral density of process n
T = Fourier series period
T_1 = see Fig. (5)
$\bar{T}$ = nonzero range of $c(t)$
$X(\omega)$ = Fourier transform of $x(t)$
$x(t)$ = nonstationary excitation process
$y(t)$ = nonstationary linear system response process
$\langle \ldots \rangle$ = ensemble average
α = see Eq. (16)
Δf = frequency increment
Δt = time increment
ε = total error in estimation of $c(t)$
ζ = damping ratio
μ = see Eq. (29)
ν = variability error
σ_n = standard deviation of process n
$\Phi_x(t, \omega)$ = instantaneous spectral density
$\phi_x(t, \tau)$ = nonstationary autocorrelation [see Eq. (6)]
ω_d = damped natural frequency
ω_n = natural frequency
ω_0 = see Eq. (16)
$\hat{\omega}$ = see Eq. (2)

Superscripts
$*$ = complex conjugate

Subscripts
p = periodic version
R = order of Fourier series approximation

Presented as Paper 74-137 at the AIAA 12th Aerospace Sciences Meeting, Washington, D.C., January 30–February 1, 1974; submitted February 19, 1974; revision received July 1, 1974. This research was supported by the MIT Lincoln Laboratory under sponsorship of the U.S. Air Force.

Index category: Structural Dynamic Analysis.

* Aerospace Engineer, Vehicle Dynamics Division. Associate Member AIAA.

† Curator, Department of Science and Technology, National Air and Space Museum.